Modelling of air pollution dispersion in Santiago de Chile

Rainer Schmitz[a,b,*]

[a]*Departamento de Geofísica, Universidad de Chile, Blanco Encalada 2085, Santiago, Chile*
[b]*Institute for Meteorology and Climate Research, Atmospheric Environment Research (IMK-IFU), Forschungszentrum Karlsruhe GmbH, Kreuzeckbahnstr. 19, 82467 Garmisch-Partenkirchen, Germany*

Abstract

In Santiago de Chile air quality standards are frequently exceeded during both summer and winter time. The evaluation of the temporal and spatial evolution of the chemical and physical characteristics of these air pollution problems requires the application of three-dimensional models. In this work, the Chilean Air Pollution Dispersion Model (CADM), a three-dimensional Eulerian chemical transport model is presented. The model is applied for the simulation of air pollution dispersion during summer. Carbon monoxide (CO) dispersion is studied in order to evaluate advection and diffusion as simulated by CADM and to characterise dispersion patterns in the Santiago basin. Horizontal and vertical dispersion patterns are presented, explaining how pollutants are ventilated out of the Santiago basin. Also, the role of turbulence on the pollutant distribution is discussed. Furthermore, an attempt is made to explain how pollutants are accumulated in the basin during night in the nocturnal stable planetary boundary layer and what mechanisms affect the transport of pollutants under these conditions. Comparing results from model simulations with observations, it can be shown that the model is able to represent the diurnal cycles of CO reasonably well. It can be concluded that CADM is suited for the application of air pollution dispersion in the Santiago basin in particular and complex terrain in general.

Keywords: Santiago de Chile; Complex terrain; Carbon monoxide; Nocturnal boundary layer; Divergence; Dispersion

1. Introduction

In 1997, the Metropolitan Area of Santiago de Chile was declared saturated zone for carbon monoxide (CO), particulate matter smaller than 10 μm in diameter (PM10), and ozone (O_3). Whereas elevated concentrations of CO and PM10 can be observed during winter time, elevated ozone concentrations are typical around summer time. The Chilean norm of an hourly average of ozone of $160\,\mu g\,m^{-3}$ is exceeded at least at one monitoring station inside the city at about 40% of the days per year. The reasons of these high ozone concentrations lie in the anthropogenic emissions of the more than 5 million inhabitants of Santiago and the photochemical activity, driven by the intense global radiation at this latitude (33°27′S). The dispersion of primary and secondary contaminants is strongly influenced by the highly complex terrain surrounding the Santiago basin.

Despite the imminent air pollution problems, the inhabitants of Santiago are facing, little research has been carried out on the spatial and temporal evolution of such air pollution episodes. Ihl (1999) described some

*Corresponding author. Departamento de Geofísica, Universidad de Chile, Blanco Encalada 2085, Santiago, Chile. Fax: +49 8821 183243.

E-mail address: schmitzr@dgf.uchile.cl.

meteorological and chemical features of the Santiago basin by means of analysing observations during summer. However, it was stressed in her work that there exists a lack of three-dimensional meteorological and chemical information. Rappenglück et al. (2000) conducted a photochemical field experiment at two sites (city centre and suburban) in Santiago, characterising the evolution of photochemical smog episodes. They concentrated on the description of the relationships between specific non-methane hydrocarbons and other precursors and their impact on the formation of photooxidants.

Gallardo et al. (2002) and Olivares et al. (2002) applied a three-dimensional model for the simulation of SO_x dispersion in Central Chile. In their work, they focused on high air pollution episodes in winter time at the regional scale. However, the resolution of 0.1° of the model applied seemed to be too coarse for the simulation of some of the meteorological features due to topographic effects.

No work has been published so far on the three-dimensional dispersion of contaminants in the Santiago basin. However, in order to understand air pollution in complex terrain as encountered in the vicinity of Santiago, such three-dimensional information seems to be very important. In this work, the Chilean Air Pollution Dispersion Model (CADM), a three-dimensional Eulerian photochemical transport model and its application to air pollution dispersion (application without chemistry) in the Santiago area is presented.

The application of the model should answer the following questions: What are the preferred patterns of air pollutant transport in the Santiago basin? To what extent are pollutants ventilated out of the basin during the day and how do they accumulate in the basin at night? What is the influence on turbulence on the pollutant distribution in the basin? These questions exclusively concern dispersion and not chemistry. Therefore, only the dispersion of CO without any chemical reaction has been considered in this first model application. Of the routinely monitored chemical substances in Santiago, CO is the only one which can be considered non-reactive on the time scales of interest (1 day). In this work, the dispersion of CO was simulated for the entire month of January 2002.

In the next section a model description is given. Section 3 gives details on the necessary model inputs. Section 4 describes model simulations and in Section 5 conclusions are drawn.

2. Model

CADM is a comprehensive, three-dimensional, multilayer, Eulerian atmospheric chemical transport model, designed to simulate relevant physical and chemical processes in the troposphere. Although it is not restricted to any particular region, the model has been developed focusing on the Metropolitan Region around Santiago de Chile. The model consists of two main modules, the mesoscale meteorological model PSU-NCAR MM5 (Grell et al., 1994) that provides all the meteorological input, and the chemistry-transport module (CTM). The MM5 provides the time-dependent three-dimensional wind, temperature, pressure, and specific humidity fields. The CTM is driven off-line by the meteorological output of the MM5 and predicts the time-varying trace gas concentrations by solving numerically a species continuity equation that includes advection, diffusion, deposition, gas and aqueous phase conversion according to

$$\frac{\partial\langle c_i\rangle}{\partial t} = -\frac{\partial}{\partial x_j}(\bar{u}_j\langle c_i\rangle) + \frac{\partial}{\partial x_j}\left(K_{jj}\frac{\partial\langle c_i\rangle}{\partial x_j}\right) + R_i(\langle c_1\rangle,\ldots,\langle c_n\rangle,T,p) + E_i(\mathbf{x},t) - S_i(\mathbf{x},t), \quad (1)$$

where c_i stands for the concentrations of a chemical species i, u_j is the velocity component in direction j, K_{jj} is the *eddy diffusivity* , R_i is the chemical generation term for i (which depends generally on the temperature, T, and at times on the pressure, p), and E_i and S_i are the emission and removal fluxes, respectively, which depends on time, t, and space, $\mathbf{x}$. A different notation for the mean values of the velocities, $\bar{u}$, and the concentrations, $\langle c_i\rangle$, is used here. Mean velocities represent a temporal and spatial average, whereas the $\langle c_i\rangle$ represents a theoretical ensemble average.

The dry deposition flux of a species i is based on a resistance model. The chemistry is dealt with by means of the chemical mechanism RADM2 (Stockwell et al., 1990). However, since neither dry deposition nor chemistry are used in this work, no further explanation of how the model treats these processes is given here.

2.1. Eddy diffusivities

The horizontal diffusive fluxes are assumed to be small and are set to zero in the current set-up. Only the vertical turbulent mixing is accounted for. In the actual version of the CTM, two possible schemes for the calculation of the vertical eddy diffusivity, K_{zz}, can be chosen from, a mixing length scheme using profile functions of Dyer (1974) and a second scheme which takes advantage from meteorological models which give information on the turbulent kinetic energy (TKE). The MM5 can be run using a 1.5-order closure scheme that explicitly predicts TKE (Shafran et al., 2000). The eddy diffusivity is then a function of TKE according to

$$K_{zz} = l_h TKE^{1/2}, \quad l_h(l_n, TKE, N^2, S^2) \quad (2)$$

and the mixing length scale, l_h is defined by Ballard et al. (1991), where l_n is again the basic length scale according

to Blackadar (1962), N is the Brunt–Väisälä frequency, and S is the vertical shear.

2.2. Numerical treatment

The CTM uses the same σ vertical coordinates as the MM5, defined as follows:

$$\sigma = \frac{p - p_{\text{top}}}{p_{\text{surf}} - p_{\text{top}}}, \tag{3}$$

where p_{surf} is the surface pressure, p_{top} is the pressure surface which defines the model top (100 mb), and p is the pressure at the level where σ is evaluated. The CTM coordinate system is staggered in the vertical and horizontal, which allows flux terms involving derivatives to be calculated compactly and accurately.

Two advection schemes can be used in the CTM. One is based on Smolarkievicz (1983), the other one on Bott (1989a, b). Both schemes can be characterised as positively definite, conservative, and computationally efficient. The diffusion term is calculated by the stable semi-implicit Crank–Nicolson method, applying twice a Gaussian elimination. The lower boundary condition of the diffusion term is represented by the dry deposition fluxes.

For the numerical solution of Eq. (1), the CTM applies an operator splitting (e.g. Seinfeld and Pandis, 1998), where first the one-dimensional terms of the advection are solved, using a symmetric splitting scheme, and afterwards the diffusion term.

The CTM has been fully parallelised for the use on multi-processor machines at low costs, using the single-instruction-multiple-data (SIMD) methodology implemented via the Message Passing Interface (MPI) standard.

2.3. Model set-up

Four nested domains were defined for the MM5 for this study. The outer domain covers an area of 2700×1782 km in the subtropical South America and the southeast Pacific. The horizontal grid spacing for each domain is 54, 18, 6 and 2 km, respectively. All four domains have 30 vertical sigma levels, with a higher resolution in the boundary layer (9 levels below 1000 m above ground level) and with the lowest sigma level at about 17 m above ground level. MM5 allows the user to choose among different parameterizations for the subgrid-scale processes. In this simulation the following parameterizations were used: a simple ice microphysics (Dudhia, 1989), a cloud radiation scheme (Dudhia, 1989), and the Gayno–Seaman boundary layer parameterization (Gayno et al., 1994). Also, the Kain–Fritsch convective parameterization was used for the two outermost domains (Kain and Fritsch, 1990), whereas for the other two domains it is assumed that convection is reasonably well resolved by the explicit microphysics (e.g. Seaman and Michelson, 2000).

To drive the CTM, the innermost domain of MM5 was used. This domain of MM5 with a resolution of 2 km has 73×100 points which apart from the Santiago basin include large parts of the Andes mountains. Such a large domain is necessary for the meteorology simulations in order to eliminate any boundary effect due to the Andes mountains on the circulation in the Santiago basin. However, since not all of this innermost domain of the MM5 seemed to be of interest for the dispersion simulation, only a part of its meteorological output fields were used to drive the CTM. This resulted in a domain of the CTM of 72×72 points maintaining the horizontal resolution of 2 km. The orographic details of the CTM model domain are given below. The same vertical layers were used in the CTM as in the MM5 simulations. For the horizontal advection in the CTM the numerical scheme according to Smolarkievicz (1983) was used and for the vertical advection the scheme according to Bott (1989a, b). The eddy diffusivities were calculated applying the TKE scheme.

3. Input data

The model system requires various input data. In the following, the data which are used in this study are described.

3.1. Initial and lateral boundary conditions

Global analyses of the NCEP (1.25° of horizontal grid spacing) were interpolated to be used as initial and boundary conditions for the MM5 simulation.

As for the MM5, the CTM needs initial and boundary conditions. Considering the limited area of the model application with its horizontal extension of $144\,\text{km} \times 144\,\text{km}$, a mean zonal wind of $5\,\text{m s}^{-1}$ would mean that air masses move over the area in less than 8 h. Hence, for limited areas of this size the lateral boundary conditions are very important. Unfortunately, apart from the measuring sites in Santiago there is very little information available on the chemical composition of air masses in and around the Santiago basin. Therefore, no assumptions, based on observations, can be made for the boundary conditions. This fact is certainly of higher importance when photochemical reactions are considered rather than inert or almost inert substances. In this study a constant background value of $0.1\,\text{mg m}^{-3}$ of CO at the lateral inflow boundaries is assumed which is also constant with height. Considering the high emissions of up to about $70\,\text{g km}^{-2}\,\text{s}^{-1}$ in some parts of downtown Santiago, the lateral boundary conditions should not have a major influence on the concentrations inside the modelled domain. Also, due to the lack of information

on the spatial distribution of CO in the Santiago basin, a constant three-dimensional field of 0.1 mg m^{-3} of CO is taken as initial condition. The first 24 h of the simulation are not taken into account for analysis since they are considered to be influenced by the (artificial) initial condition.

3.2. Topography

The left panel of Fig. 1 shows the topography of the modelled domain of the CTM. The domain covers an area of 144 km × 144 km. The data are plotted with the same horizontal grid intervals (2 km × 2 km), as used in the CTM simulations. Also the location of Santiago is pointed out, as given by the land use data. It can be seen that the Santiago basin is confined by the Andes mountain range to the east with mountains, according to the topography used in the model, of an altitude up to about 4800 m and to the west by a coastal mountain range up to about 1600 m. Indicated in Fig. 1 are the Mapocho valley northeast, the Maipu valley southeast, and the Camino a Melipilla southwest of Santiago. The right panel of Fig. 1 zooms in the panel of the left-hand side in order to indicate the measuring sites in Santiago with their respective letters, as used in the monitoring network.

3.3. Emission data

The emission inventory of Santiago is based on three source groups: mobile, point and area sources. According to this inventory around 90% of the CO emissions come from mobile sources (traffic), with the remaining 10% from point and area sources. Due to the high contribution of the mobile sources to the total, the emissions have a distinct diurnal cycle (Fig. 2), following traffic activity. This cycle which has a temporal resolution of 1 h is applied over the entire model domain, with the amplitude depending on traffic intensity in the respective area. The emission inventory is available at a horizontal resolution of 2 km × 2 km which corresponds to the horizontal grid interval of the model domain. The daily average for a weekday of the CO emissions in the basin are also shown in Fig. 2. Apart from Santiago there are no significant CO sources in the basin.

4. Model simulations

4.1. Time period

The time period chosen for the model simulation was January 2002. First MM5 was run and then its hourly output data were then used to drive the CTM for the whole month. During the summer months Central Chile is generally under the influence of the subtropic anticyclone in the Southeastern Pacific (with weak pressure gradients on the synoptic scale), resulting in clear sky and high temperatures in Santiago. The wind patterns at the meso-γ-scale are mainly influenced by topographic effects during this time. The results obtained for January 2002 are therefore expected to be representative for a month in summer in general since the main forcing of the basin circulations is certainly governed by topographical features. At 20 days in January 2002, ozone exceeded the norm of 160 μg m^{-3} over 1 h average. However, no particular synoptic situation could be singled out for these events. Considering these two points—that wind patterns on the meso-γ-scale are mainly controlled by topographic effects and that no particular synoptic situation seems to be responsible for summer smog episodes—the following results of the model simulations are, without exception, presented as averages of the whole month of January 2002. These averages are assumed to be representative for air pollution dispersion during summer time in the Santiago basin.

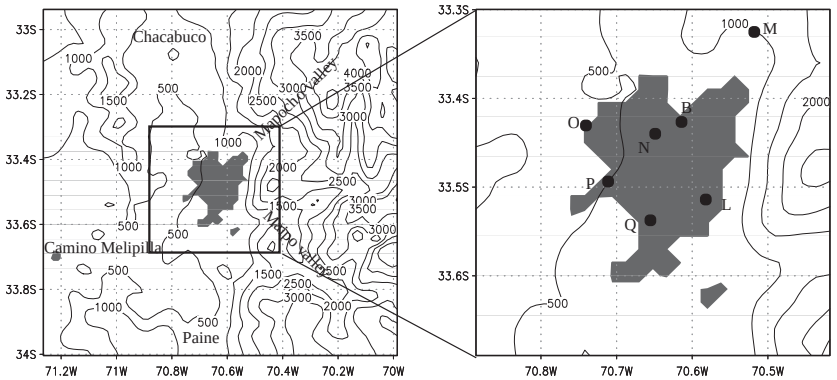

Fig. 1. Topography of the model domain with 500 m contours. The right panel indicates the location of the measuring sites with their respective letters, as used in the monitoring network. The shaded area represents urban land use as represented in the model.

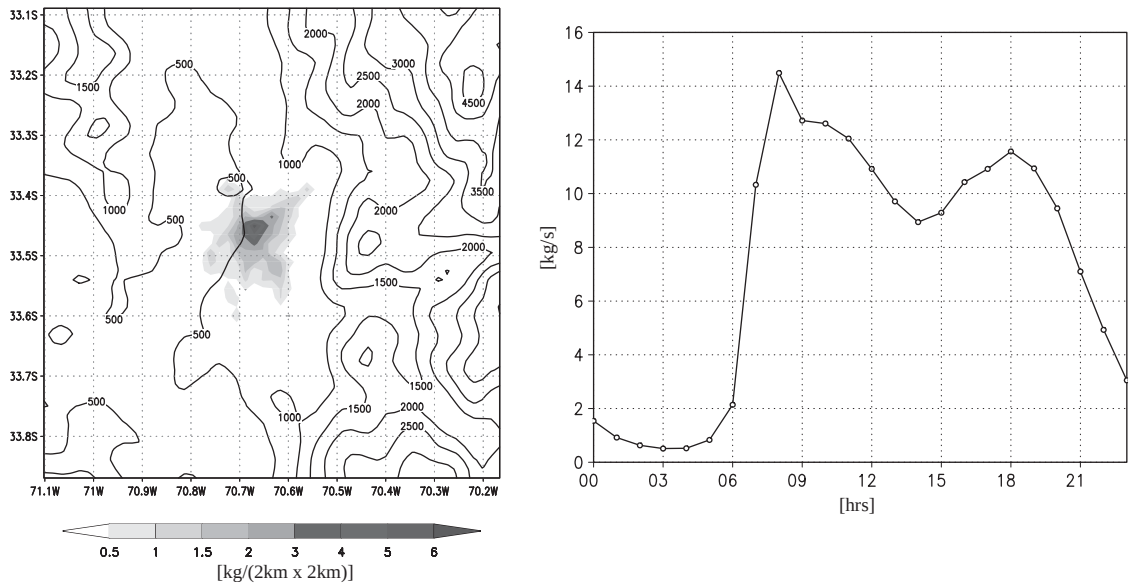

Fig. 2. Emission patterns in Santiago. The left panel shows the daily averaged emissions for a weekday in January. The solid lines indicate the topography. The right panel indicates the diurnal cycle of emission rate, integrated over the entire model domain. Times are given in local hour.

Table 1
Mean statistical performance measure of the fourth domain of MM5 at all surface stations

	RMSE WD		RMSE WS		ME WD		ME WS	
Local time	04	16	04	16	04	16	04	16
Mean	87	24	0.7	1.4	−12	6	0.2	−0.6

4.2. Meteorology

During the night regime (0000–0600) (all hours given in local time strong down-slope and down-valley winds can be observed) in the Andes mountains. They get significantly weaker as soon as they reach more or less the 1000 m isoline east of the basin. Down-slope winds can also be observed in the coastal mountain range but with much less intensity. In the basin itself winds are very weak and little organised. In contrast, during the day regime the wind patterns are very organised due to the pronounced up-slope and up-valley winds. During this regime southwesterly winds prevail in the basin with increasing southerly components from south to north. In the Andes mountains and the coastal mountain range the wind patterns are governed by topographic effects characterised by up-valley and up-slope winds. The transition phases from night to day (0600–1200) and day to night regime (1800–2400) can generally be described as transition from down-slope and down-valley to up-slope and up-valley winds and vice versa, respectively, and in the basin in particular from little organised to organised and vice versa, respectively. It is not in the scope of this work to make a detailed statistical analysis of the meteorology simulation compared with observation. Therefore, only global statistical data are given in Table 1, representing average values for all meteorological stations in the basin (a total of 15). Table 1 shows values for the root mean square error (RMSE) and the mean error (ME) for the wind speed (WS) and the wind direction (WD) at 2 h representing night (0400) and day (1600) conditions. The model performance at night is relatively poor which is reflected in the high values of the WD-RMSE at 0400 LT as compared to those at 1600 LT. On average, the daytime WS-RMSE values are about twice the nighttime values. However, since wind speeds are more than five times higher during daytime the WS-RMSE relative to the wind speed is larger during nighttime.

4.3. Horizontal dispersion

Fig. 3 shows average surface wind and CO concentration fields in the Santiago basin. The solid lines indicate the topography. It should be noted that although the graphs display the mentioned fields at the indicated time,

the CO concentrations have not been influenced by the wind fields at that instance of time, but represent the evolution of the wind and therefore the concentration fields *until* that time. Whereas from a meteorological point of view the graphs had to be interpreted in terms of day and night regime and their respective transition phases from a dispersion and air pollution point of view the emissions have to be taken into account also.

Traffic activity starts between 0500 and 0600 (see Fig. 2). At this time, winds are very weak and the atmosphere is statically stable down to the surface (see below). Very little dispersion seems to occur in large parts of the city. Yet, due to prevailing northeasterly winds southwest of the city (see wind patterns at 0600) there exists some extension of CO concentrations towards the Camino a Melipilla (see concentrations at 0900) due to advection. However, generally speaking, it can be said that little horizontal dispersion exists around the hour of the emission maximum. Dispersion increases with the development of the up-slope and up-valley winds between 0900 and 1200 and, of course, the onset of turbulence (see below). With the development of the unstable diurnal PBL and therefore increasing turbulence, CO concentrations drop significantly during the day. Due to prevailing southwesterly winds in the area of Santiago, the dispersion plume is directed towards the

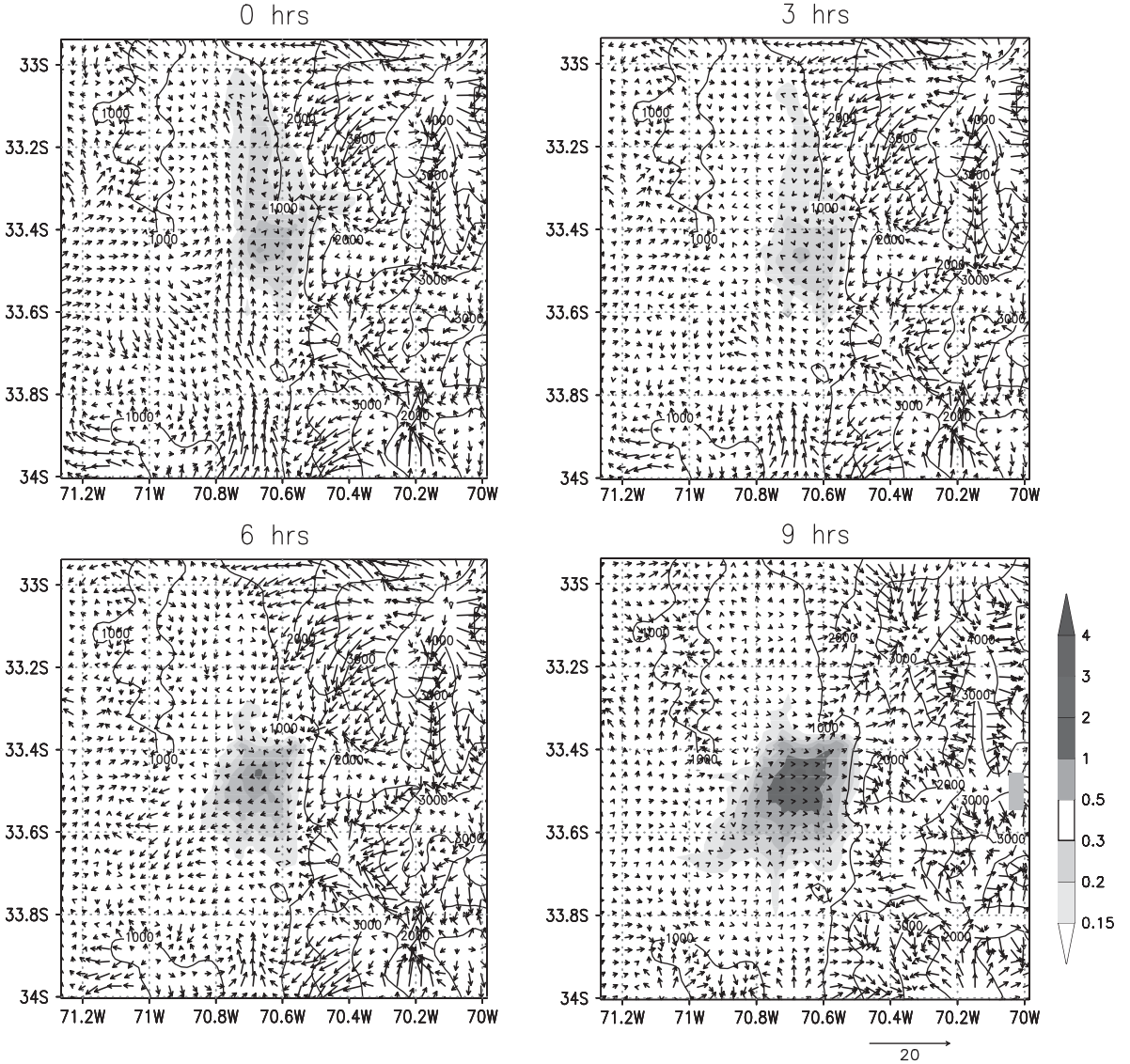

Fig. 3. Surface winds and CO concentrations. Solid lines indicate the topography. Times are given in local hour.

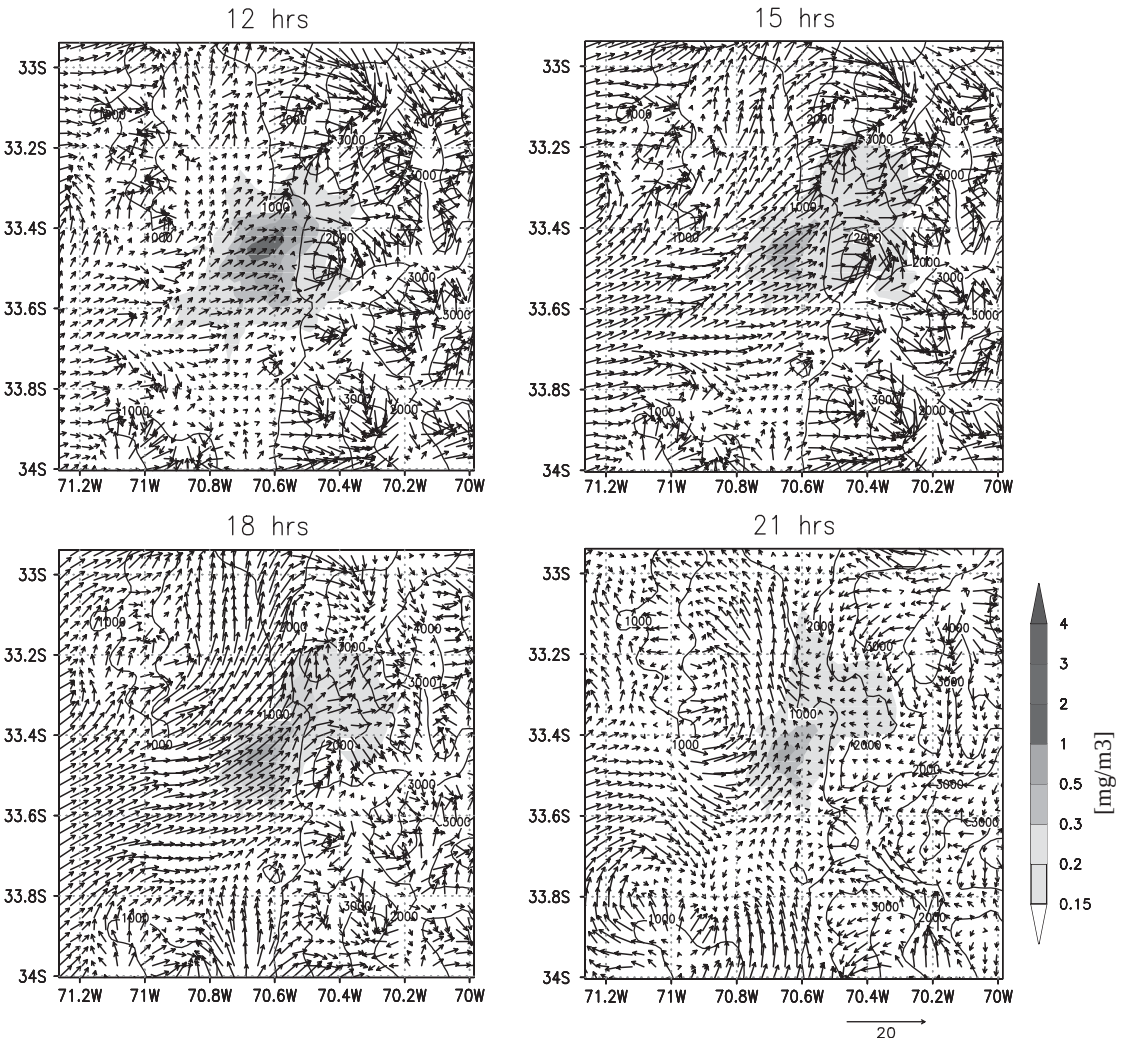

Fig. 3. (*Continued*)

Mapocho valley (see concentrations at 1200, 1500, and 1800). Having once reached the Andes mountains, the dispersion of CO is controlled by topographic effects. Immediately after sunset starts the transition phase from day to night regime. In the Andes mountains, the winds change rapidly from up-slope and up-valley to down-slope and down-valley winds. In the basin a relative increase of the southerly component of the winds which influence the dispersion of contaminants increase whereas the wind's magnitude decreases (see 1800, 2100, and 2400). At 2400 the dispersion plume is directed towards north of the city. Recirculation from the Andes mountains seem to contribute to this plume (see 2100). The elongated shape of the plume towards north, trapped to the Andes mountains is characteristic during night. Very weak northerly winds north of the city (see 0300), advect part of this plume back to the city.

4.4. Vertical dispersion

Fig. 4 shows average cross-sections at 33.45°S, interpolated to pressure levels. The solid lines represent potential temperature. They clearly show the commence of the unstable planetary boundary layer (PBL) in the basin at very low levels in the morning (see 0900). The mixing layer height reaches on average a maximum in the simulations of about 1800 m in the afternoon. Towards sunset this height decreases (see 1800) and the PBL becomes stable towards midnight (see 2100 and 2400). In the Andes mountains this diurnal cycle is much less pronounced and the unstable PBL never develops to such an extent as in the basin. Traffic activity starts in the morning when the PBL is stable in the basin confining contaminants close to the ground level (see 0600 and 0900). Due to the development of the unstable

PBL, contaminants are transported aloft by turbulence (see 1200) and with the development of the up-slope winds they are also advected towards the Andes mountains (see 1500 in Figs. 3 and 4). In Fig. 4, slightly elevated concentrations can be observed at 1500 at about 70.4°W. Comparing Figs. 4 and 3, it can be seen that these concentrations are transported from Santiago north eastwards to the Mapocho valley and from there due to topographic effects southwards to the latitude of Fig. 4. The concentrations aloft at this point might be explained by turbulence and also convergence (see below). In the basin, due to suppressed turbulence little vertical dispersion can be observed during the night (see 1800–0600). However, since the decrease of the unstable PBL height coincides with little CO emissions, this does not result in elevated concentrations at the surface. It is also worth noting that during all day and night in the basin the highest concentrations aloft can be observed towards the Andes mountains. Whereas during day this can be explained by the interaction of turbulence and advection, at night the responsible mechanism for this seems to be convergence. This shall be explained in the next section. Generally, it has to be stressed that vertical measurements of chemical and meteorological variables are needed in future in order to validate these vertical dispersion profiles.

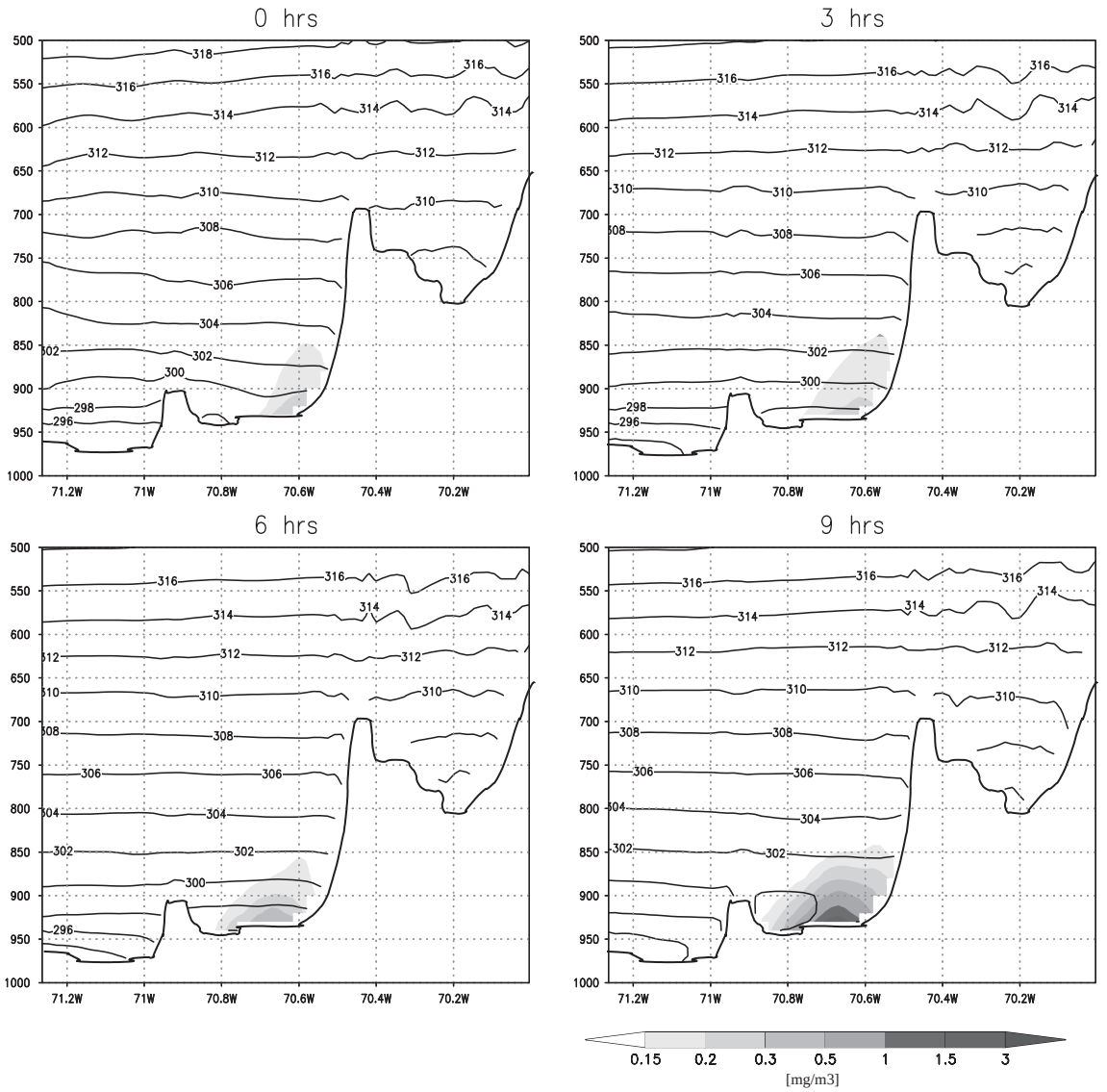

Fig. 4. Cross-section of CO concentrations interpolated to pressure levels at 33.45°S. Solid lines represent potential temperature in *K*. Times are given in local time.

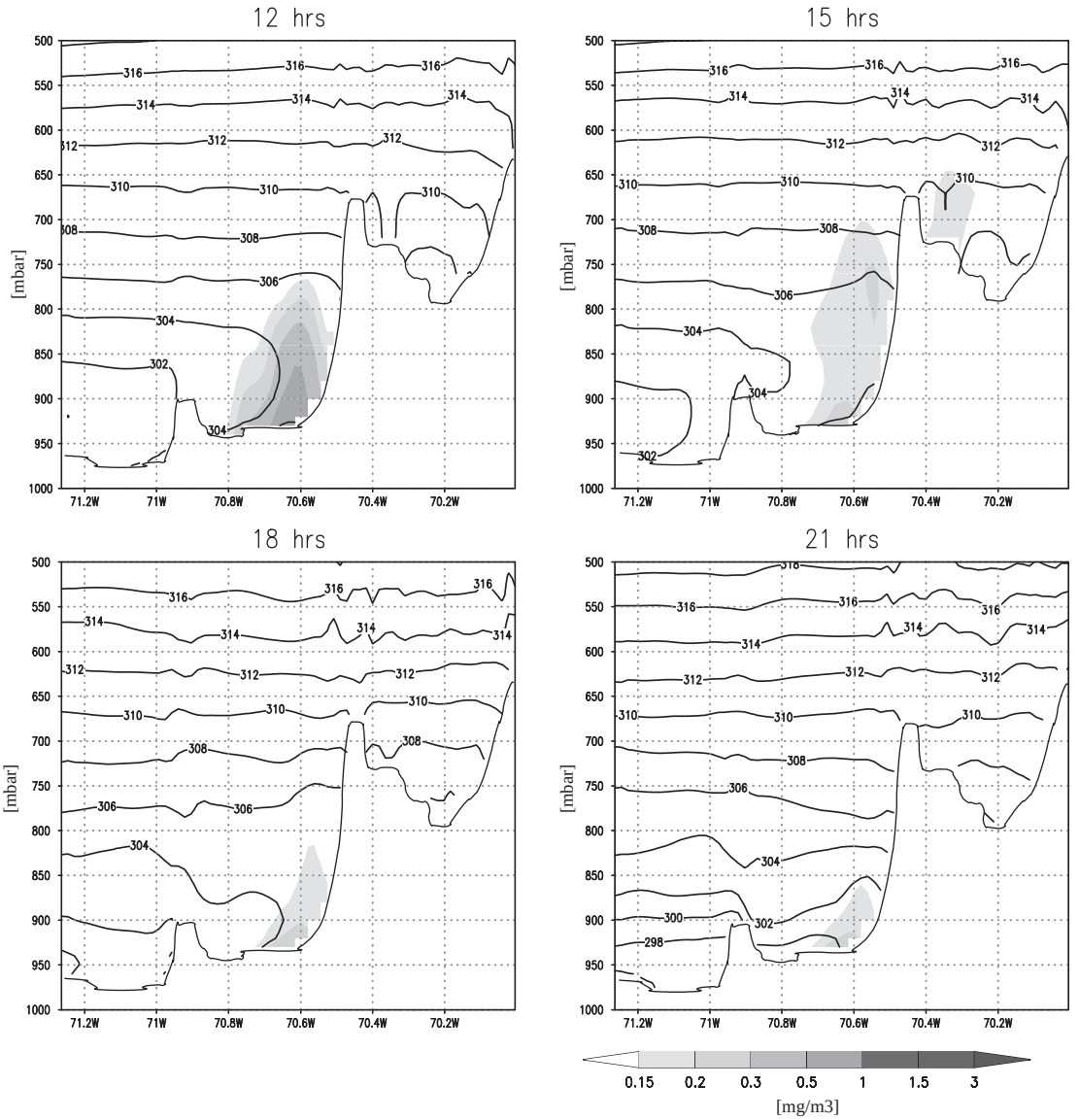

Fig. 4. (*Continued*)

4.5. Divergence and convergence

Fig. 5 shows the divergence in the Santiago basin (70.4–71.2°W, 33.2–33.8°S) for the night (0000–0600) and day regime (1200–1800). Comparing the two regimes and considering the wind pattern for day and night (Fig. 3), it can be seen that the down-slope winds cause divergence (during night time) and the up-slope winds convergence (during day time) at the top of the mountains, whereas in the valleys the opposite effect can be observed. A change from convergence to divergence zones from day to night can also be observed in the basin. The patterns inside the basin can be described as "bands" which alternate between convergence and divergence. The strong convergence of up to $-4 \times 10^{-3}\,s^{-1}$ during the day at the top of the mountains may cause transport of contaminants aloft even in a diurnal stable PBL. During the night, the persistent convergence and divergence zones in the basin might also influence the transport of contaminants. Due to the interaction of advection, turbulence, and emission this contribution is difficult to quantify at day as well as at nighttime. However, since in the stable nocturnal stable PBL turbulence is highly surpressed and therefore convergence may substantially contribute to the vertical transport of contaminants during this regime, it would

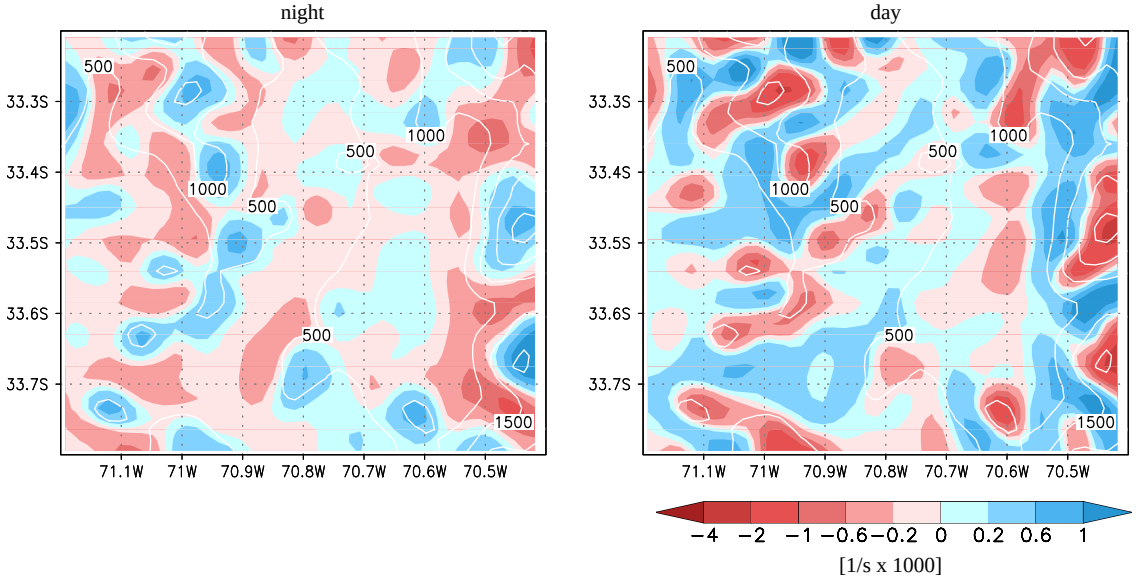

Fig. 5. Divergence during the night and the day regime.

be very interesting to have at least qualitative estimation of this contribution. For this purpose, an experiment with the following characteristics was carried out:

(a) The same meteorological fields of January 2002, as described above, were used.
(b) Zero emissions were applied.
(c) Vertical diffusion was set to zero.
(d) Every day at 0000 the surface concentrations were set to unity and at all other vertical levels to zero.
(e) The model was integrated from 0000 to 0600 for all 31 days of January 2002.
(f) Finally, only the concentration fields at 0600 were analysed. These fields are assumed to represent the integrated effect of vertical transport due to divergence/convergence during night.

By resetting the concentration fields to the initial conditions as given in (d) the influence of divergence/convergence during the night can be evaluated without the fields being influenced by any transport during daytime or the transition regime. Fig. 6 shows the average cross-sections of the resulting 31 concentration fields at 0600 at different latitudes. It can be clearly seen that a significant vertical transport exists in the convergence zones at all the latitudes shown. The vertical transport at about 77.55°W at all latitudes corresponds to the convergence zone trapped to the Andes mountains. This explains the higher concentrations aloft towards the Andes mountains at night, as mentioned in the section before. Also, the divergence zones can be clearly identified at all latitudes as zones where concentrations are low from aloft down to the surface. This can be explained by the downward transport of (artificially) clean air from higher to lower levels. The very strong vertical transport at 33.6°S/70.5°W and 33.7°S/70.5°W can be attributed to the convergence due to drainage flows in the valley. Whereas the statistical measures of wind direction showed a relatively poor performance at night, this experiment under artificial conditions still suggests that convergence plays an important role during the stable nocturnal regime regarding the vertical transport of contaminants.

4.6. Comparison of simulation and observation

A comprehensive comparison between simulations and observations would require results from an extense field campaign with measuring sites outside the urban and suburban area, downwind of emission sources and ideally vertical measurements. However, so far no measuring campaigns with the objective of characterising air pollutant dispersion have been carried out in the modelled area. Hence, only surface data from the monitoring network of Santiago are used in this study. As shown in Fig. 1, most stations in this network are located in urban areas. Urban stations are usually less suited for comparison between observations and simulations since they might be influenced by local effects on the subgrid scale which are not necessarily accounted for in the model. This would certainly be the case to a lesser

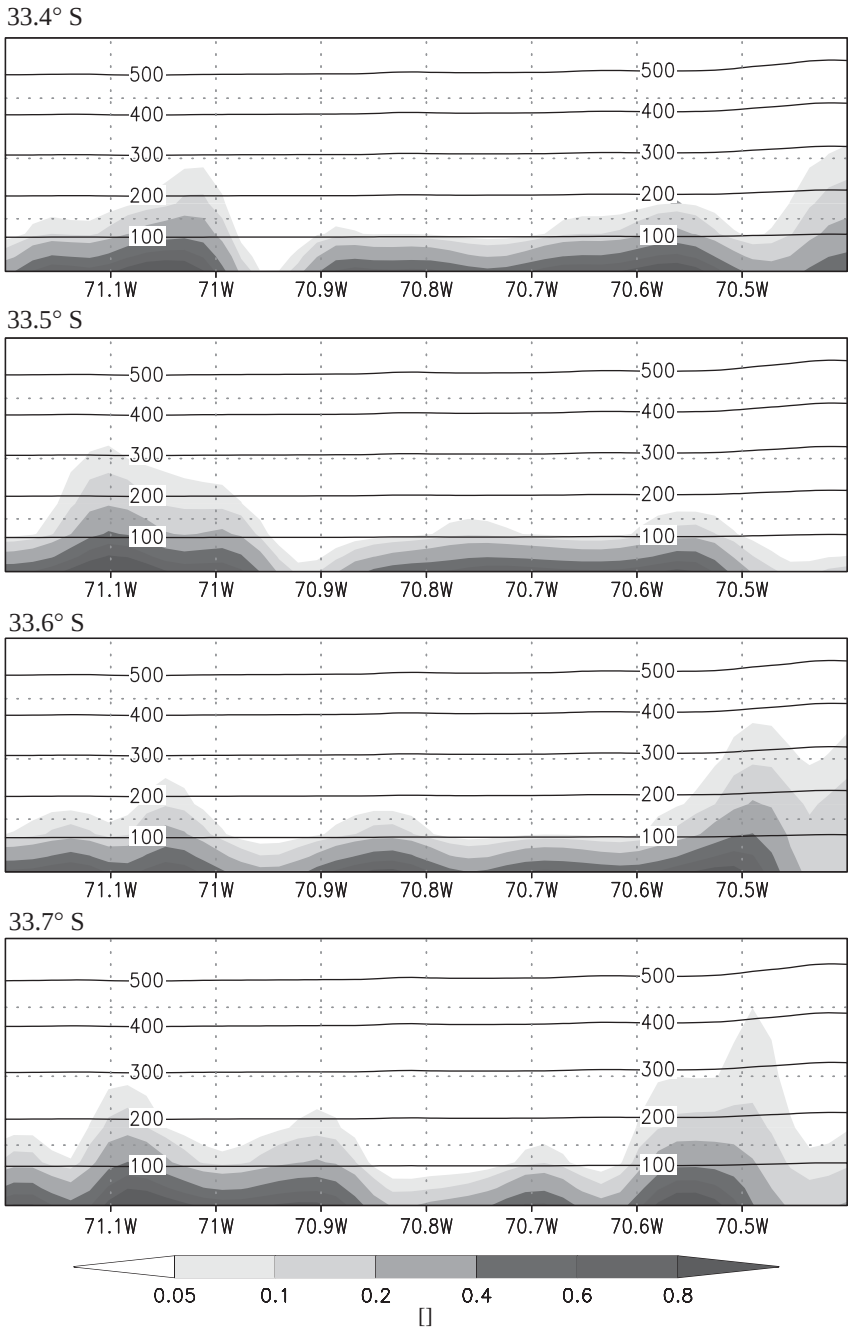

Fig. 6. Cross-section of concentration fields at 33.4°S, 33.5°S, 33.6°S, and 33.7°S for an idealised experiment neglecting vertical diffusion. Also indicated are the respective heights in m. The concentrations are given in unity.

extent for secondary (e.g. ozone) than it is for primary (e.g. CO) pollutants. Local effects on the subgrid scale are, to some extent, present at all the measuring sites in Santiago. In the following, a statistical analysis of the model results is given. Furthermore, an attempt is made to explain some of the model shortcomings qualitatively.

Table 2 provides quantitative information on statistical measures, following some recommendations of Willmott (1982). The statistical variables given are observed mean, $\bar{O}$, model-predicted mean, $\bar{P}$, standard deviation of observed values, σ_o, standard deviation of model-predicted values, σ_p, mean absolute error, MAE,

Table 2
Quantitative measures of the CO dispersion as predicted by the CADM model for January 2002

Station	$\bar{O}$	$\bar{P}$	σ_o	σ_p	MAE	RMSE	r
B	0.50	0.70	0.52	0.56	0.19	0.61	0.43
O	0.23	0.25	0.21	0.16	0.03	0.21	0.39
N	0.18	0.93	0.33	0.90	0.76	1.11	0.48
M	0.39	0.24	0.20	0.18	0.15	0.29	0.13
L	0.56	0.32	0.41	0.23	0.25	0.49	0.19
Q	0.45	0.36	0.43	0.35	0.09	0.50	0.20
P	0.10	0.42	0.22	0.43	0.32	0.50	0.43

rootmean square error, RMSE, and correlation coefficient, r. (For the definitions of the statistical variables see e.g. Willmott, 1982.)

Observed and model-predicted mean values exhibit generally an acceptable agreement. The two notable exception are the stations N and P. These sides exhibit the lowest $\bar{O}$ values of all stations. On the other hand, the $\bar{P}$ values are relatively high for station P and very high for N. The difference between $\bar{O}$ and $\bar{P}$ are by far the greatest for station N. According to the emission inventories, this site lies within an area of very high emissions (see also Figs. 1 and 2). The effect of these relatively high emissions is noted in the high model-predicted value particularly during the morning hours at around 0900 (not shown here) when, due to little dispersion, the pollutants accumulate close to their sources. The fact that this is not reflected in the observed values might be explained by local effects: Station N is located close to a highway and a major urban road. Depending on the wind direction this station lies downwind (generally in the early morning hours) or upwind (in the late morning hours and in the afternoon) of these emission sources and therefore seems to receive contaminated or relatively clean air masses, respectively. This local effect would not be taken into account by the model. This observation would again stress the limited use of urban stations for a comprehensive comparison between observations and model predictions.

From Table 2 it appears that station O shows the best agreement between observations and model predictions with respect to the means, their standard deviation, MAE, and r. (The relatively large difference between MAE and RMSE, however, indicates a high over-prediction of extreme values.) This station generally lies upwind the emission sources (see Fig. 3). On the other side of the city, station M also shows good agreement between observations and model predictions with respect to the means, their standard deviation, MAE, and RMSE. However, there exists a very low correlation between observations and model predictions.

As mentioned before, the statistical performance of wind directions, as simulated by MM5, at night is rather poor. It should be expected that this poor performance should also affect the statistical performance of the CTM. However, since emissions and therefore concentrations are very low at night, most of the statistical variables used in this study will be mainly affected by the daytime values. For example the average MAE of all stations between 0000 and 0600 is 0.04 compared to 0.26 during the whole day. Also, it can be assumed that the night errors do not have a major impact on the day performance considering that the first-order forcing during the day are the very high emissions.

Finally, it has to be said for a more rigorous evaluation of the model performance information from more suburban sites and vertical measurements would be necessary.

5. Summary

The chemical transport model CADM, consisting of the meteorological mesoscale model MM5 and a photochemical transport module CTM, has been presented. The model has been developed for simulations of photochemical air pollution in complex terrain.

The MM5 run for January 2002 shows that the model is able to reproduce the main surface features of the spatial and temporal variations of the daytime thermally driven circulations in the Santiago basin. Surface wind directions and speeds are well simulated especially under conditions of a well-developed thermally driven flow. During nighttime, wind speeds are reasonably well represented by the model, whereas wind directions are poorly simulated.

The CTM has also been applied for January 2002 driven by the MM5 meteorological outputs for the simulations of the dispersion of CO in the Santiago basin, assuming that this month is characteristic for summer time air pollution dispersion. CO was chosen since it is not very reactive and routinely monitored at most measuring sites in Santiago. By means of model simulations, the horizontal and vertical dispersion patterns have been identified. It can be concluded that in the Santiago basin during summer at daytime most of the contaminants are transported towards the northeast

of the city into the Mapocho valley and ventilated out of the basin by up-slope winds over the Andes mountains. During nighttime, the region north of the city is mostly affected.

Whereas it could be shown that turbulence controls vertical dispersion during the day, it could also be shown that divergence and convergence may play an important role in the vertical dispersion at night when convergence zones seem to contribute effectively to the transport of contaminants aloft. Due to extreme topography of the model domain, further investigation of divergence and convergence should be of general interest.

Considering the inherent problems of modelling CO dispersion (particularly local effects), it could be shown that the results from the model simulations agree reasonably well with observations.

Generally, it has to be stressed that this work should contribute to further research efforts in order to understand air pollution in Santiago. As a next step, the simulation of photochemical contaminants such as ozone is necessary. Yet, the results shown in this work may directly be used as a basis for the design of future measuring campaigns in the area. For such campaigns the inclusion of measuring sites outside the city and downwind the emissions, according to the presented results, are necessary.

Acknowledgements

This work was financed by CONAMA. The author wishes to thank M. Uhlmann from the Potsdam Institute for Climate Impact Research, Germany, for his most valuable help in the parallelisation of the model code. H. Jorquera and J. Castro provided the emission data. Discussions with R. Rondanelli and H. Fuenzalida were a great help to improve this work.

References

Ballard, S., Golding, B., Smith R., 1991. Mesoscale model experimental forecasts of the haar of northeast scotland. Monthly Weather Review.

Blackadar, A., 1962. The vertical distribution of wind and turbulent exchange in a neutral atmosphere. Journal of Geophysical Research 67, 3095–3102.

Bott, A., 1989a. A positive definite advection scheme obtained by nonlinear renormalization of the advection flux. Monthly Weather Review 117, 1006–1015.

Bott, A., 1989b. Reply. Notes and correspondence. Monthly Weather Review, 117, 2633–2636.

Dudhia, J., 1989. Numerical study of convection observed during the Winter Monsoon experiment using a mesoscale two-dimensional model. Monthly Weather Review 46, 3077–3107.

Dyer, A., 1974. A review of flux-profile relationships. Boundary-Layer Meteorology 7, 363–372.

Gallardo, L., Olivares, G., Langner, J., Aarhus, B., 2002. Coastal lows and sulfur air pollution in central chile. Atmospheric Environment 36, 3829–3841.

Gayno, G.A., Seaman, N.L., Lario, A.M., Stauffer, D.R., 1994. Forecasting visibility using a 1.5-order closure boundary layer scheme in a 12-km non-hydrostatic model. 10th Conference on Numerical Weather Prediction, American Meteorological Society, Portland, OR, pp. 18–20.

Grell, G., Dudhia, J., Stauffer, D., 1994. A description of the 5th-generation Penn State/NCAR mesoscale model (MM5). Technical Report, NCAR Technical note TN-398 + STR.

Ihl, M., 1999. La dinamica espacio-temporal del smog de verano en Santiago de Chile. Ph.D. Thesis, University of Bern, Switzerland (in Spanish).

Kain, J.S., Fritsch, J.M., 1990. A one-dimensional entraining/detraining plume model and its application in convective parameterization. Journal of Atmospheric Science 47, 2784–2802.

Olivares, G., Gallardo, L., Langer, J., Aarhus, B., 2002. Regional dispersion of oxidized sulfur in central chile. Atmospheric Environment 36, 3819–3828.

Rappenglück, B., Oyola, P., Olaeta, I., Fabian, P., 2000. The evolution of photochemical smog in the metropolitan area of Santiago de Chile. Journal of Applied Meteorology 39, 275–290.

Seaman, N., Michelson, S., 2000. Mesoscale meteorological structure of a high ozone episode during the 1995 NARSTO-Northeast study. Journal of Applied Meteorology 39, 384–398.

Seinfeld, J., Pandis, S., 1998. Atmospheric Chemistry and Physics. Wiley, New York.

Shafran, P., Seaman, N., Gayno, G., 2000. Evaluation of numerical predictions of boundary layer structure during the lake michigan ozone study. Journal of Applied Meteorology.

Smolarkievicz, P., 1983. A simple positive definite advection scheme with small implicit diffusion. Monthly Weather Review 111, 479–486.

Stockwell, W., Middleton, P., Chang, J., Tang, X., 1990. The second generation regional acid deposition model chemical mechanism for regional air quality modeling. Journal of Geophysical Research 95, 16,343–16,368.

Willmott, C.J., 1982. Some comments on the evaluation of model performance. Bulletin of the American Meteorological Society 63, 1309–1313.